

# Damage Detection for CFRP Based on Planar Electrical Capacitance Tomography

Wenru Fan and Chi Wang\*

College of Electronic Information and Automation, Civil Aviation University of China, Tianjin, 300300, China

\*Corresponding Author: Chi Wang. Email: chi.wang@foxmail.com

Received: 22 April 2020; Accepted: 29 July 2020

**Abstract:** Due to the widespread use of carbon fiber reinforced polymer/plastic (CFRP), the nondestructive structural health monitoring for CFRP is playing an increasingly essential role. As a nonradiative, noninvasive and nondestructive detection technique, planar electrical capacitance tomography (PECT) electrodes array is employed in this paper to reconstruct the damage image according to the calculated dielectric constant changes. The shape and duty ratio of PECT electrodes are optimized according to the relations between sensitivity distribution and the dielectric constant of different anisotropic degrees. The sensitivity matrix of optimized PECT sensor is more uniform as the result shows, because the sensitivity of insensitivity area can be increased by adding rotation of optimized electrodes. The reconstructed image qualities due to different PECT arrays and different damage locations are investigated at last. The simulation results indicate that: PECT can be used to detect the surface damage of CFRP; the sensitivity matrix of PECT for CFRP is highly relevant with the degree of anisotropic dielectric constant; the rotatable PECT sensor with rotation has better performance in uniformity of sensitivity; for different damage locations, the rotatable sensor with rotation has better image quality in most cases.

**Keywords:** Planar electrical capacitance tomography (PECT); carbon fiber reinforced polymer/plastic (CFRP); damage detection; image reconstruction

## 1 Introduction

Carbon fiber reinforced polymer/plastic (CFRP) is widely used in aerospace field, defence industry and other high-tech industries for its high strength to weight ratio, corrosion resistance and so on. In some field, the CFRP is taking the place of metal to play the role of structural support. However, damage may occur during manufacturing and use. Therefore, the nondestructive test (NDT) for the CFRP in service is essentially. Various of NDT techniques including acoustic emission [1,2], ultrasound [3,4], X-ray [5,6], and thermography [7,8] have been proposed to detect the damage of CFRP. However, the above methods are based on different types of extensive human involvement, expansive procedures or radiation.

CFRP is made up of carbon fiber and resin, which means the conductivity and dielectric constant are highly correlated with damage [9]. Conductivity of CFRP is widely investigated, because the dielectric constant is not significant for the conductive material in the previous investigation. But the insulating



This work is licensed under a Creative Commons Attribution 4.0 International License, which permits unrestricted use, distribution, and reproduction in any medium, provided the original work is properly cited.

layer of CFRP have to be removed in order to decrease the contact resistance for the conductivity detection, which means CFRP would be damaged during conductivity detection. For the past few years, as the developing of PECT detection method and the investigation of the dielectric constant [10–12] of CFRP, the techniques for CFRP detecting based on dielectric constant are gradually improved. The techniques for CFRP detecting based on dielectric constant are mainly capacitive imaging (CI) and PECT. The detection principle of CI and PECT are similar, which reflect the changes of dielectric constant by the measured capacitance. The difference between CI and PECT are the number of electrodes and image reconstruction method [13–15]. The electrodes of CI are only two and the image is directly reconstructed by the measured capacitance. Diamond et al. [16] adopted circle electrode to detect the impact damage of CFRP, the hole of thermalite block and the hidden delaminations of a tiled flooring sample. The result shows that CI has the potential to detect dielectric constant changes of samples. Yin et al. [17,18] optimized the shape and relative position of CI electrodes according to the image reconstruction contrast of different shape and the sensitivity distribution of electrodes, respectively. In addition, they investigate the lift-off effect of CI and the detection capability of various materials based on their back-to-back triangle electrode [19–24]. However, the electrodes of PECT are array and the image of PECT are reconstructed by some algorithms.

The CI is simple than PECT in image reconstruction, but the drive mechanism is complicated and it takes a lot of time for each conduction. For PECT, many investigations based on isotropic materials [25–27] has been conducted as well. Several electrodes array such as square electrodes array [28], two-plate square electrodes array [29], fan-shaped electrodes array [30] and mixed in many shapes electrodes array [31] has been studied for the detection of metal knife, damages, landmine, flora et.al. On this basis, planar electrodes array is a potential tool to detect damages of CFRP by reflecting the changes of capacitance. Nevertheless, the existing investigations on PECT are mainly based on the isotropic materials. Therefore, the research focus on the anisotropic materials is essentially. In this paper, sensitivity analysis based on anisotropic materials is conducted and the electrodes array is optimized according to analysis results.

The main contributions in this paper are summarized as follows. Firstly, planar electrodes array is utilized to detect the damage of CFRP. Secondly, the detecting ability of planar electrodes array is investigated for different degrees of anisotropic property (ratio of axial to radial dielectric constant) of CFRP. Thirdly, the shape and duty ratio of electrodes are improved according to the sensitivity distribution. Fourthly, the image qualities due to different damage locations are analyzed by simulation.

## 2 PECT Detection Method for CFRP

The electrodes structures for ECT and PECT are different. In traditional ECT, the fringe effect can be ignored for its subtle influence. However, as Fig. 1 shows, the fringe effect is employed in PECT sensors due to the in-plane location of electrodes to detect the dielectric constant change of a material under test (MUT).

### 2.1 Principle of PECT

The principle for PECT is similar to ECT which can be described by the forward problem and inverse problem.

The forward problem can be addressed by setting geometry giving, the boundary conditions, and assuming the dielectric constant distribution. The formula for PECT can be described as

$$\nabla \cdot (\boldsymbol{\varepsilon} \nabla \mathbf{u}) = 0 \quad (1)$$

where  $\boldsymbol{\varepsilon}$  is the dielectric constant in the study region, and  $\mathbf{u}$  is the electric potential distribution. Capacitance between driving electrode and sensing electrode is obtained by

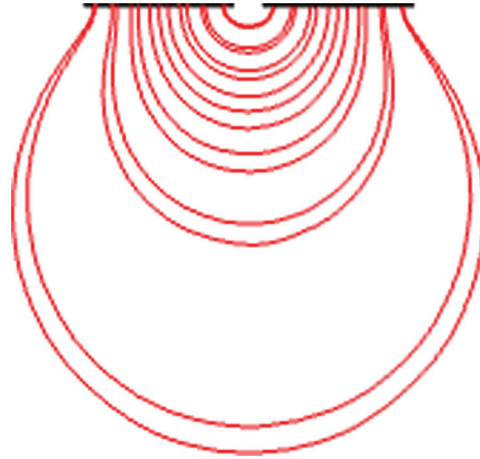


**Figure 1:** The fringe effect between planar sensors

$$C = \frac{Q}{V} = - \iint_{\Gamma} \varepsilon(x, y) \nabla u(x, y) d\Gamma \quad (2)$$

where  $C$  is the calculated capacitance,  $V$  is the potential difference between driving electrode and sensing electrode, and  $\Gamma$  is the surface of sensing electrode. The finite element formula of Eq. (2) can be expressed as

$$\lambda_{M \times 1} = \mathbf{S}_{M \times N} \mathbf{g}_{N \times 1} \quad (3)$$

where  $\lambda$  is the reconstructed vector of capacitance,  $\mathbf{S}$  is the sensitivity matrix,  $\mathbf{g}$  is the vector of dielectric constant,  $M$  is the number of measurements, and  $N$  is the number of pixels in the reconstructed image. The sensitivity matrix can be calculated by

$$S_{i,j} = - \iint_p E_i \cdot E_j dx dy \quad (4)$$

where  $S_{i,j}$  is the sensitivity in the pixel  $p$ ,  $E_i$ ,  $E_j$  are the electric field value under excitation of  $i$ -th,  $j$ -th electrode, respectively.

The inverse problem of PECT is to estimate the unknown dielectric constant distribution by the capacitance measurements. As the excitation and sensing pattern, the single electrode excitation pattern is employed. When the electrode 1 (E1) is chosen to be exciting electrode, E2-E16 are grounded. Then the capacitance is measured from E2-E16. When E2 is excitation electrode, E1 and E3-E16 is grounded. Then the capacitance is measured from E3-E16. By that analogy, 120 capacitance measurements can be obtained. When the sensitivity matrix and capacitance are all obtained, the dielectric constant changes can be calculated by some image reconstruction algorithms. The commonly used method including non-iterative 2-norm regularization method such as Tikhonov algorithm (Tikh), iterative 1-norm regularization method such as L1 regularization algorithm (L1), and other iterative method such as conjugate gradient least squares (CGLS). In the following investigation, both Tikh, L1 and CGLS are taken into consideration.

## 2.2 The Finite Element Model of CFRP and Square PECT Electrodes Array

The structure of CFRP can be divided into unidirectional CFRP  $[0^\circ]$ , orthogonal CFRP  $[0^\circ/90^\circ]$  and cross CFRP  $[0^\circ/45^\circ/-45^\circ/90^\circ]$  according to the different laying directions of carbon fibers. Here, the

orthogonal CFRP is the research subject. As Fig. 2 shows, the finite element model for CFRP is set up by COMSOL Multiphysics 5.4. The length and width are all set to 100 mm, and the thickness of CFRP is set as 2.1 mm including two insulation layers and ten fiber layers. The thickness of insulation layer is 0.05 mm and each fiber layer thickness is 0.2 mm. According to [10], the dielectric constant is set as 2160 and 1640 for axial direction and radial direction of carbon fiber, respectively.

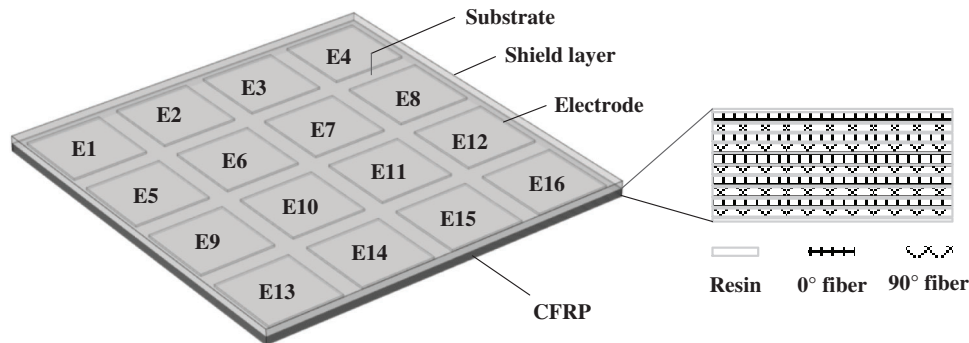


**Figure 2:** The finite element model of CFRP

The PECT sensor is made up of electrodes, substrate and shield layer on the top. The size of PECT substrate is  $100 \times 100 \times 2$  mm and the size of each electrode is  $20 \times 20 \times 0.1$  mm. In addition, the thickness of shield layer is 0.1 mm.

### 2.3 The Sensitivity Matrix of PECT for CFRP

The electric potential can easily pass through the insulator, but it could not pass through the good conductor. The surface layer of CFRP is insulator, but the fiber layer lies between conductor and dielectric material. To analyze the detection capabilities of PECT for CFRP, 2 dimensional (2D) finite model is built with 2 kHz alternating current (AC) excitation. As Fig. 3 shows, only if the damage layer is near the electrodes, the damage can be detected clearly. The damage away from the electrodes is hardly to be detected. In this way, the PECT detection method can be considered as a surface detection method.

Therefore, the sensitivity matrix just need to be calculated in the fiber layer near electrodes. However, the dielectric constant may change due to the different kinds of carbon fiber, resin and volume ratios of fiber to resin. To investigate the performance of PECT under different anisotropic degrees, the dielectric constant of radial direction are set to 1640 (low anisotropic degree) and 35 (high anisotropic degree), respectively. In Fig. 4, it can be observed that the maximum sensitivity value of each excitation and sensing is higher at the edge of electrodes and the value is very low at the interval, when the dielectric constant of radial direction is set to 35. However, the result is completely opposite, when the dielectric constant of radial direction is set to 1640. It means that the damage may not be detectable when the damage located under the electrodes and intervals, while the dielectric constant of radial direction is set to 1640 and 35 respectively. In other words, the degree of anisotropy have big influence on the detection sensitivity. When the anisotropic degree is high, the higher sensitivity value concentrate under the edge of the electrodes. When the anisotropic degree is low, the higher sensitivity value concentrate at the intervals. Therefore, the sensor structure of PECT should be adjusted according to the degree of anisotropy.

In the following investigation, the constant of radial direction is set to 1640 according to [10], which means the higher sensitivity value appears in the interval of electrodes.

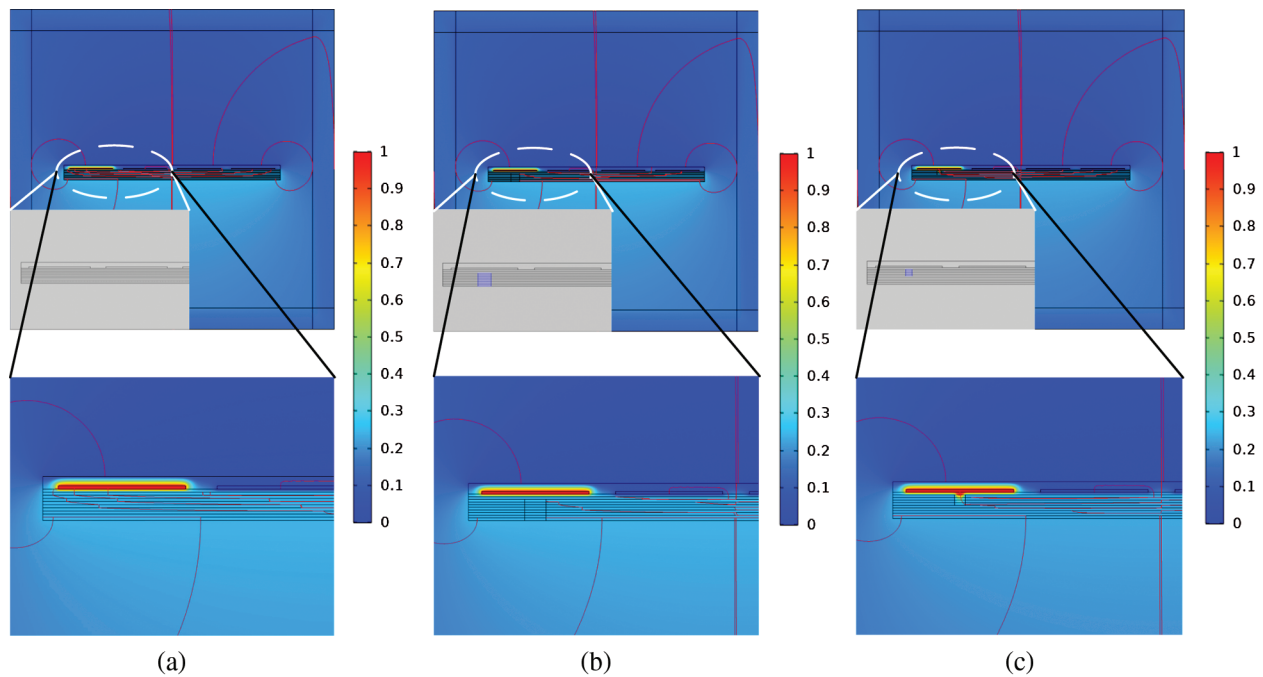


**Figure 3:** Electric potential and electric field distribution for CFRP before and after different damage (a) Without damage (b) Damage far away from electrodes (c) Damage layer next to electrodes (apart from insulation layer)

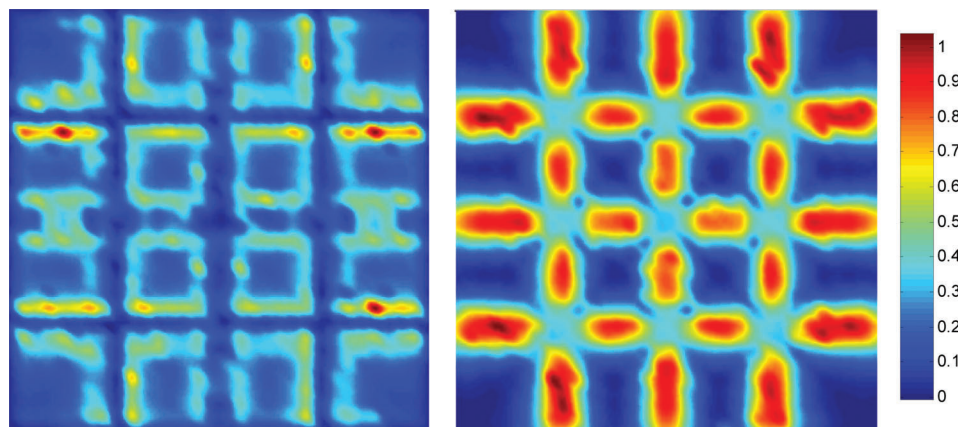


**Figure 4:** The sensitivity distribution when the dielectric constant of radial direction is set to 35 (left) and 1640 (right), respectively

#### 2.4 Rotatable Electrodes Design

No matter what kind of dielectric constant is set, the square PECT sensor have its insensitivity region under the electrodes or at the interval. Therefore, a new PECT sensor which can decrease the insensitivity region of sensitivity matrix is designed to detect the damage of CFRP. In this paper, a fan-shaped electrode structure, as Fig. 5 shows, is employed due to its rotatable property. To increase the detection area, the electrodes are arranged in two circles. In each detection, as shown in Fig. 5(b), the

measurements for capacitance are conducted twice for the electrodes before and after rotation. In this case, the insensitivity region is drastically reduced for both higher and lower anisotropic degrees.

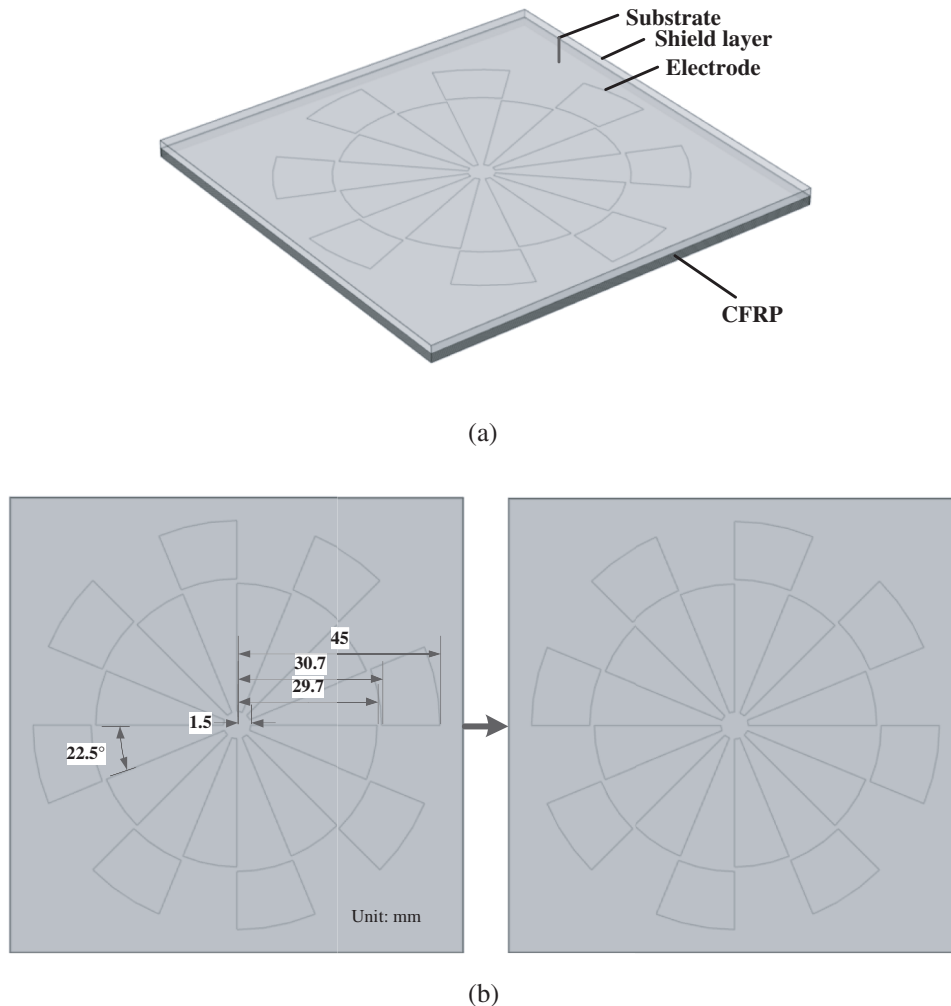


**Figure 5:** Model of rotatable electrodes (a) Rotatable sensor 3D model (b) Electrodes location before (left) and after (right) rotation

Before the electrodes rotation, the area under electrodes is insensitive. However, the areas under electrodes turn to interval when the electrodes are rotated. Therefore, the whole are becomes sensitive except for the area of center and the area between two circles. The maximum sensitivity of each excitation is drawn in Fig. 6. Due to the lower degree of anisotropy, the higher sensitivity value concentrate on the interval of sensor, which is consistent with the analysis in 2.3. However, the sensitivity distribution is more uniform when the rotated sensitivity is added. Therefore, damages at more locations can be detected.

### 3 Simulations

#### 3.1 Simulation Settings and Evaluation Index

In order to analyze the detection ability of PECT as comprehensively as possible, impact damages with different locations are employed to reconstruct the dielectric constant changes. Four damage locations are

considered including at the center (D1S, D1R), under the electrode (D2S, D21R), under the interval (D3S, D3R), and half under electrode (D4S, D4R). Then the image quality is analyzed for comparison. The simulated 3D models of impact damages are the same with Fig. 7. The reconstructed image of traditional square electrodes and new rotatable electrodes are simulated to compare the damage detection ability. The simulation is conducted by COMSOL Multiphysics 5.4 and MATLAB R2014a. The computer has an Intel(R) CORE (TM) i5-7200U CPU @2.50 GHZ and 8 GB of RAM.

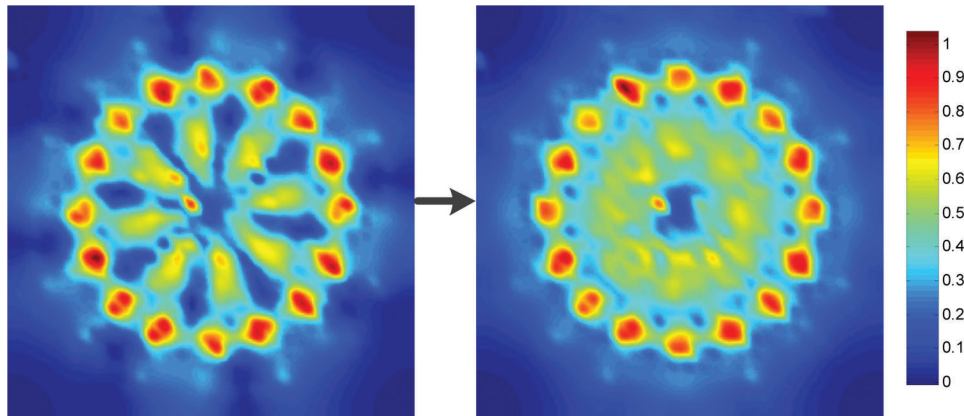


**Figure 6:** Sensitivity distribution before (left) and after (right) rotation

The commonly used Tikhonov algorithm, conjugate gradient least squares (CGLS) algorithm and L1 regularization algorithm are utilized to reconstruct the dielectric constant changes. The correlation coefficient (CC) is employed to evaluate the consistency between the real damage and the reconstructed one. The formula of CC can be written as

$$CC = \frac{\sum_{i=1}^p (\varepsilon_i - \bar{\varepsilon})(\hat{\varepsilon}_i - \bar{\hat{\varepsilon}})}{\sqrt{\sum_{i=1}^p (\varepsilon_i - \bar{\varepsilon})^2 \sum_{i=1}^p (\hat{\varepsilon}_i - \bar{\hat{\varepsilon}})^2}} \quad (5)$$

where  $\hat{\varepsilon}$  is the real distribution of dielectric constant,  $\varepsilon_i$  is the calculated one,  $\bar{\hat{\varepsilon}}$  is the average dielectric constant,  $\bar{\varepsilon}$  is the average of the calculated one.

### 3.2 Image Reconstruction and Its Quality

The reconstructed images of damage are shown in Figs. 8, 9 and 10 for the three PECT arrays, square-shaped electrodes, fan-shaped electrodes without and with rotation. The bar charts of correlation coefficient of reconstructed images are drawn in Fig. 11. In this paper, the regularization parameters are chosen by experience. The regularization parameters for Tikh and L1 are  $4 \times 10^{-2}$  and  $5 \times 10^{-10}$ , respectively. In addition, the iterations of CGLS is set as 20.

In Fig. 9, the image quality is poor when the damage occurs under the electrodes, due to the higher sensitivity value are located at the edge and intervals of electrodes. The same conclusion can be drawn for the damage D4S. For the rotatable electrodes, the image qualities are better at the interval and become worse under the electrodes as well. However, the reconstructed image have better qualities for the rotatable electrodes with rotation when the damage located under the electrodes and the interval, for the sensitivity behaves better with rotation. With regards to the part of damage under the electrodes, the image quality in Fig. 10 is better than Fig. 9, but still not good enough. In order to further improve

the image quality, multiple rotation can be conducted. The trend of bar chart in Fig. 11 are close to the visual effect of Figs. 8–10. The reconstructed images of L1 regularization perform better in EIT and ECT, but the results of L1 are close to Tikh and CGLS for PECT.

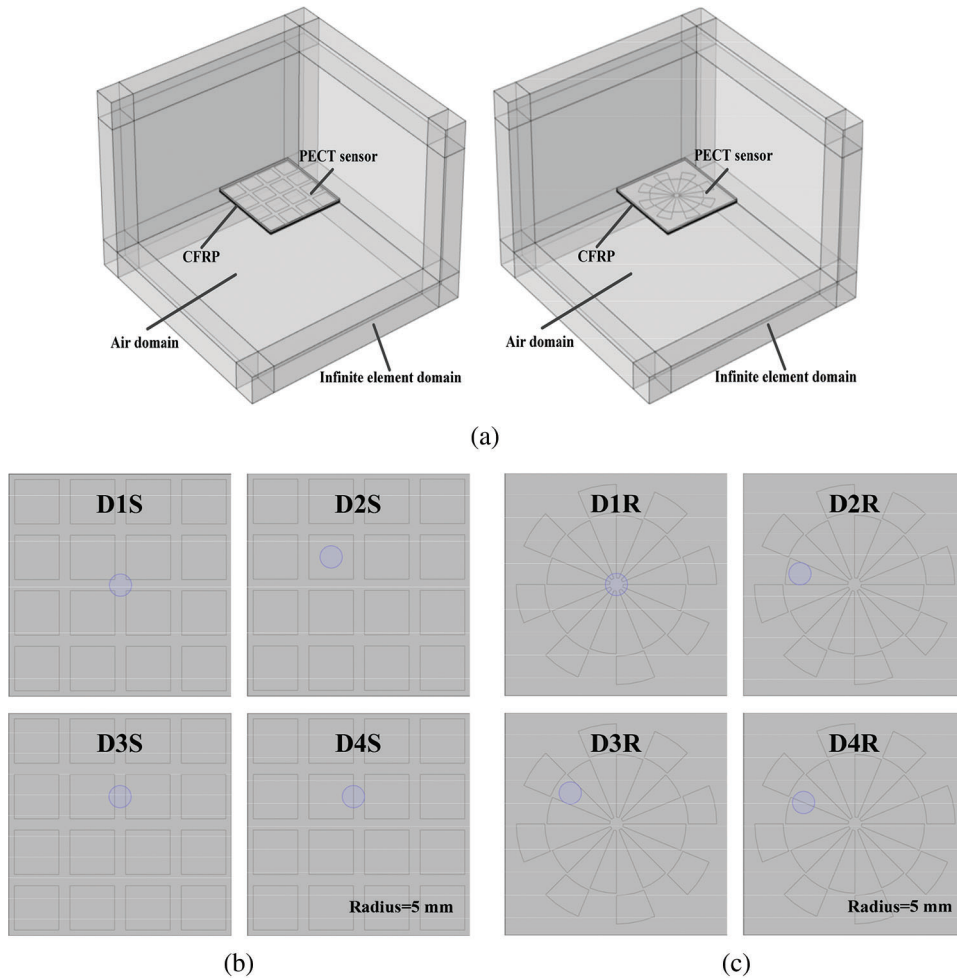


**Figure 7:** The damage models used to simulate (a) Simulated 3D models (b) Single impact damage models for the square electrode (c) Single impact damage models for the rotatable electrodes

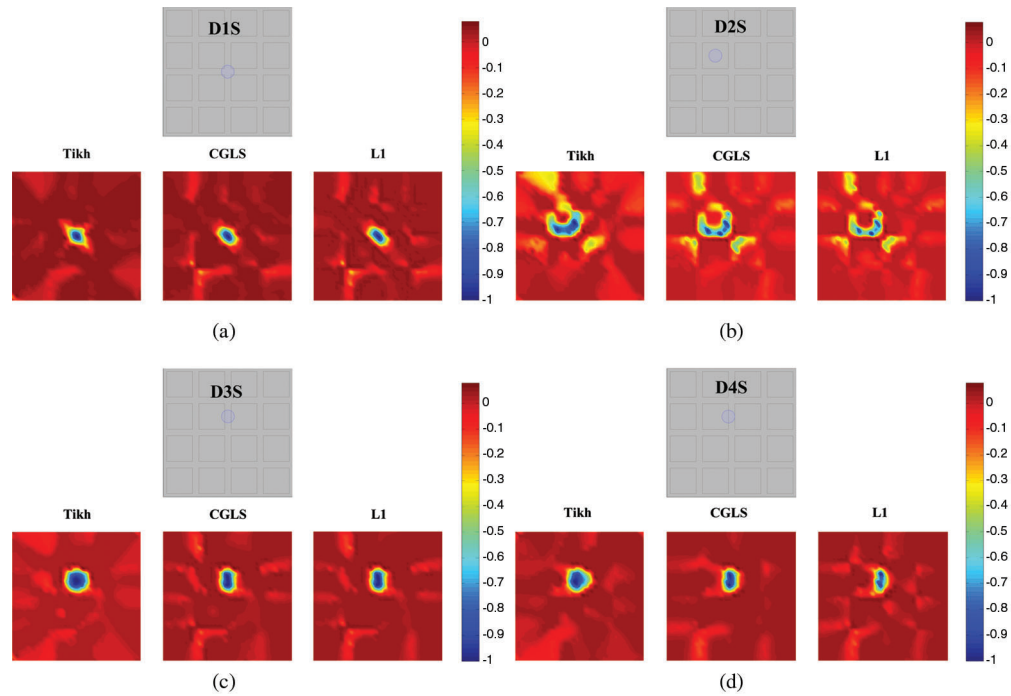


**Figure 8:** The reconstructed image of square electrodes (a) The reconstructed image of D1S (b) The reconstructed image of D2S (c) The reconstructed image of D3S (d) The reconstructed image of D4S

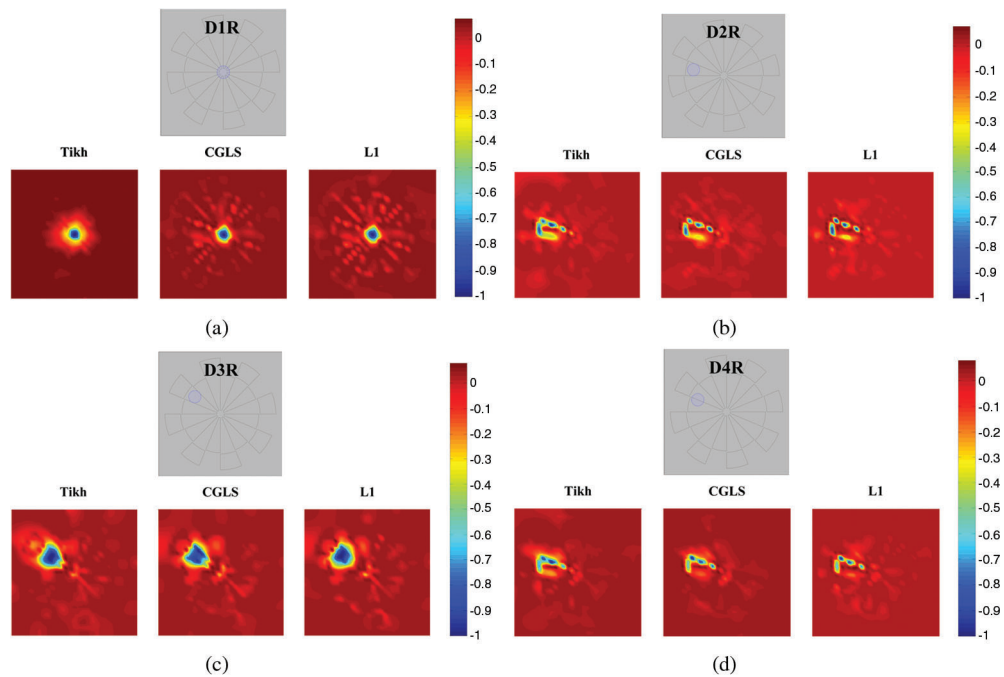


**Figure 9:** The reconstructed image of rotatable electrodes without rotation (a) The reconstructed image of D1R without rotation (b) The reconstructed image of D2R without rotation (c) The reconstructed image of D3R without rotation (d) The reconstructed image of D4R without rotation

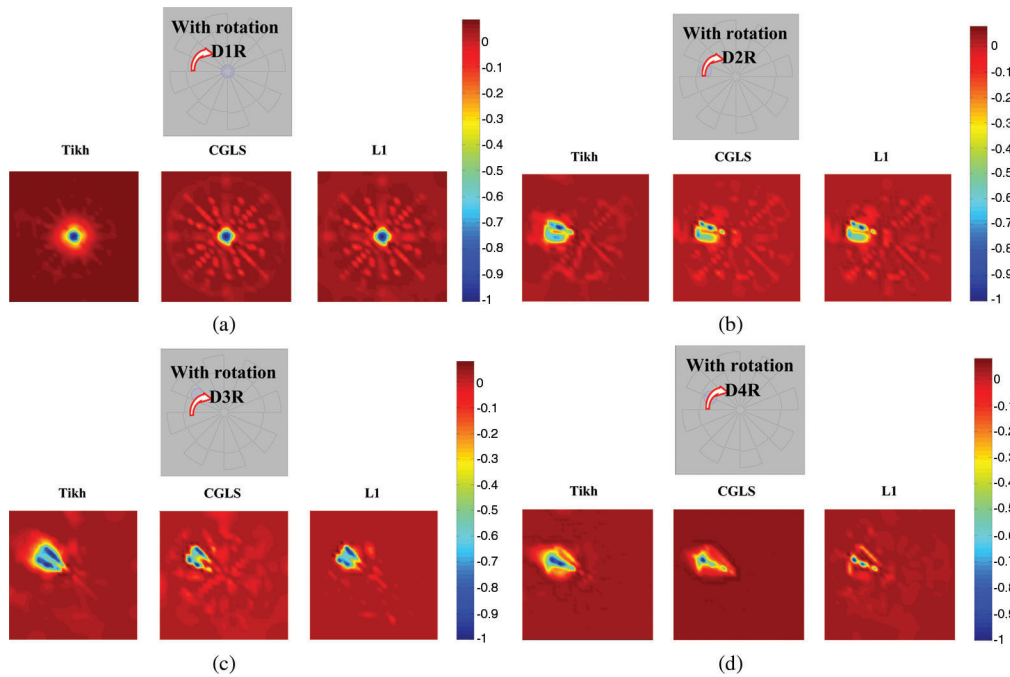


**Figure 10:** The reconstructed image of rotatable electrodes with rotation (a) The reconstructed image of D1R with rotation (b) The reconstructed image of D2R with rotation (c) The reconstructed image of D3R with rotation (d) The reconstructed image of D4R with rotation

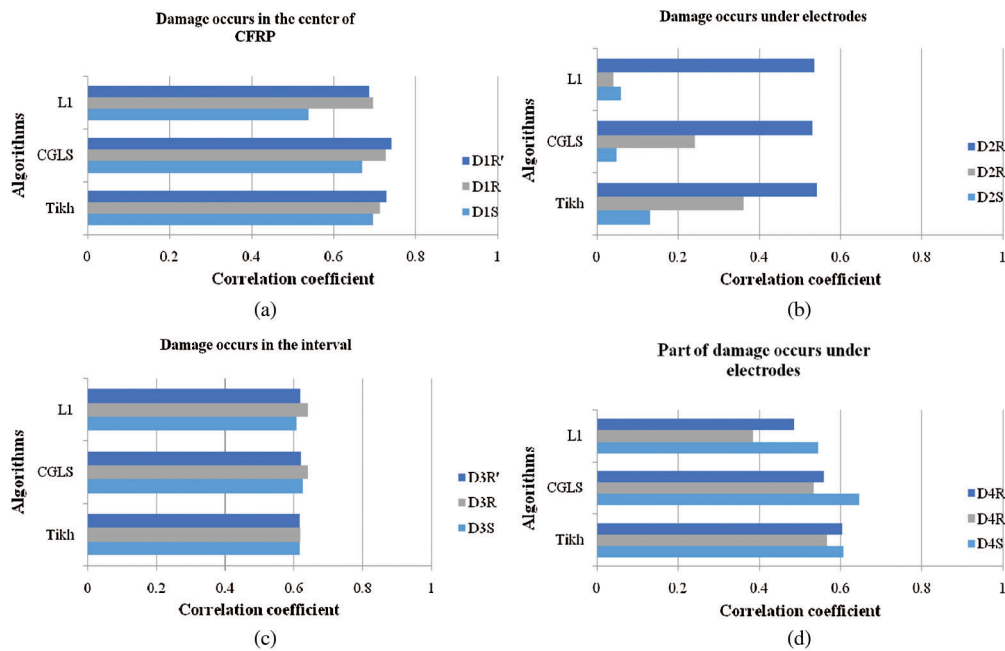


**Figure 11:** The correlation coefficient between reconstructed image and real damage distribution (a) Correlation coefficient of different algorithms when damage occurs in the center of CFRP (b) Correlation coefficient of different algorithms when damage occurs under electrodes (c) Correlation coefficient of different algorithms when damage occurs in the interval (d) Correlation coefficient of different algorithms when part of damage occurs under electrodes

#### 4 Conclusion

PECT is used to detect damages of CFRP in this paper. The structure of PECT electrodes is optimized according to the distribution of sensitivity caused by the different anisotropic degrees of dielectric constant. By adding the rotation of the optimized PECT electrodes, the sensitivity distribution is more uniform and has better reconstruction quality in visual effect and correlation coefficient. The feasibility of optimized PECT electrodes is verified by damage occurring in different locations.

Data mining of measured capacitance will be conducted to quickly determine the location and size of damage in the future works. Then, image reconstruction performed on the measured data to judge the damage from reconstructed image and information of data mining. In addition, PECT reconstruction results can be integrated with imaging results such as EIT and ECT to obtain better imaging quality. Finally, the analysis of sensitivity distribution and rotatable PECT sensor can be used to optimize the structure of PECT electrodes in other detection field with different anisotropic degrees of dielectric constant.

**Funding Statement:** This work is supported by the National Natural Science Foundation of China (Grant No. 61871379).

**Conflicts of Interest:** The authors declare that they have no conflicts of interest to report regarding the present study.

#### References

1. Leng, S., Wang, Z., Min, T., Dai, Z. Q., Chen, G. (2020). Detection of tool wear in drilling CFRP/TC4 stacks by acoustic emission. *Journal of Vibration Engineering & Technologies*, 8(3), 463–470. DOI 10.1007/s42417-019-00190-5.
2. Rescalvo, F. J., Aguilar-Aguilera, A. J., Vargas, E. S., Valverde-Palacios, I., Gallego, A. (2018). Acoustic emission during wood-CFRP adhesion tests. *International Journal of Adhesion and Adhesives*, 87, 79–90. DOI 10.1016/j.ijadhadh.2018.09.007.
3. Zeng, X., Yang, C. L., Zhou, X. J., Teng, G. Y. (2018). Ultrasonic detection of rich-resin in low-porosity CFRP. *Optics & Precision Engineering*, 26(11), 2732–2743. DOI 10.3788/OPE.20182611.2732.
4. Ribolla, E. L. M., Hajidehi, M. R., Rizzo, P., Scimemi, G. F., Spada, A. et al. (2017). Ultrasonic inspection for the detection of debonding in CFRP-reinforced concrete. *Structure and Infrastructure Engineering*, 14(6), 807–816. DOI 10.1080/15732479.2017.1384843.
5. Zhang, H. Z. (2019). Static compression testing CFRP single-lap composited joints using X-ray  $\mu$ CT. *Composite Structures*, 234, 111667.
6. Tserpes, K. I., Stamopoulos, A. G., Pantelakis, S. G. (2016). A numerical methodology for simulating the mechanical behavior of CFRP laminates containing pores using X-ray computed tomography data. *Composites Part B: Engineering*, 102, 122–133. DOI 10.1016/j.compositesb.2016.07.019.
7. Myrach, P., Maierhofer, C., Rahammer, M., Kreutzbruck, M. (2016). Parameters in lock-In thermography of CFRP laminates. *Materials Testing*, 58(1), 31–35. DOI 10.3139/120.110814.
8. Shi, Q. Z., Liu, J. Y., Liu, W. Y., Wang, F., Wang, Y. (2019). Barker-coded modulation laser thermography for CFRP laminates delamination detection. *Infrared Physics & Technology*, 98, 55–61. DOI 10.1016/j.infrared.2019.02.007.
9. Eddib, A. A., Chung, D. D. L. (2018). Electric permittivity of carbon fiber. *Carbon*, 140, 413–427. DOI 10.1016/j.carbon.2018.08.070.
10. Eddib, A. A., Chung, D. D. L. (2018). First report of capacitance-based self-sensing and in-plane electric permittivity of carbon fiber polymer-matrix composite. *Carbon*, 140, 413–427. DOI 10.1016/j.carbon.2018.08.070.
11. Xi, X., Chung, D. D. (2019). Colossal electric permittivity discovered in polyacrylonitrile (PAN) based carbon fiber, with comparison of PAN-based and pitch-based carbon fibers. *Carbon*, 145, 734–739.

12. CJunior, M. A., Gomes, N. A., Pinto, S. D., Rezende, M. C., Marcuzzo, J. S. et al. (2018). Influence of the permittivity on carbon fiber particulates applied in radiation absorbing materials. *Global Journal of Research in Engineering*, 17(8), 290903.
13. Marashdeh, Q., Teixeira, F. L., Fan, L. S. (2015). Electrical capacitance tomography. *Industrial Tomography: Systems and Applications*, 3–21. DOI 10.1016/B978-1-78242-118-4.00001-0.
14. Beck, M. S., Byars, M., Dyakowski, T., Waterfall, R. C., He, R. et al. (1997). Principles and industrial applications of electrical capacitance tomography. *Measurement & Control*, 30(7), 197–200. DOI 10.1177/002029409703000702.
15. Malcolm, B. (2001). *Developments in Electrical Capacitance Tomography*. PTL Application Notes, Hannover, Germany.
16. Diamond, G. G., Hutchins, D. A., Gan, T. H., Purnell, P., Leong, K. K. (2006). Single-sided capacitive imaging for NDT. *Insight-Non-Destructive Testing and Condition Monitoring*, 48(12), 724–730. DOI 10.1784/insi.2006.48.12.724.
17. Yin, X., Hutchins, D. A., Chen, G., Li, W. (2013). Investigations into the measurement sensitivity distribution of coplanar capacitive imaging probes. *Ndt & E International*, 58, 1–9. DOI 10.1016/j.ndteint.2013.04.001.
18. Yin, X., Chen, G., Li, W., Hutchins, D. A. (2013). Design and characterization of planar capacitive imaging probe based on the measurement sensitivity distribution. *AIP Conference Proceedings*, 1511, Melville NY, pp. 1586–1592.
19. Yin, X., Li, C., Li, Z., Li, W., Chen, G. (2018). Lift-off effect for capacitive imaging sensors. *Sensors*, 18(12), 4286. DOI 10.3390/s18124286.
20. Wen, Y. T., Jia, Y., Zhang, Y. Y., Luo, X. Y., Wang, H. R. (2016). Study on the non-destructive detection of the adhesive layer of thermal insulation material based on improved ECT. *Chinese Journal of Scientific Instrument*, 37(7), 1596–1602.
21. Chen, D., Hu, X., Yang, W. (2011). Design of a security screening system with a capacitance sensor matrix operating in single-electrode mode. *Measurement Science and Technology*, 22(11), 114026. DOI 10.1088/0957-0233/22/11/114026.
22. Leow, P. L. (2018). Planar imaging of stagnant and hydrodynamic fluid using miniaturized ECT device. *International Journal of Integrated Engineering*, 10(8), 99–102.
23. Yin, X., Li, Z., Yuan, X., Li, W., Chen, G. (2020). Corrosion depth inversion method based on the lift-off effect of the capacitive imaging (CI) technique. *IEEE Access*, 8, 22770–22779. DOI 10.1109/ACCESS.2020.2970204.
24. Fan, G., Gupta, S., Loh, K. J. (2018). Curing and subsurface damage monitoring of epoxy-based composites. *Structural Health Monitoring-An International Journal*, 18(4), 1040–1055. DOI 10.1177/1475921718776612.
25. Din, S. M., Razali, N. A. M., Pusppanathan, J., Song, C. P., Rahim, R. A. et al. (2018). Planar imaging of stagnant and hydrodynamic fluid using miniaturized ECT device. *International Journal of Integrated Engineering*, 10(8), 131–135.
26. Wen, Y. T., Jia, Y., Zhang, Y. Y., Luo, X. Y., Wang, H. R. (2017). Defect detection of adhesive layer of thermal insulation materials based on improved particle swarm optimization of ECT. *Sensors*, 17(11), 2440. DOI 10.3390/s17112440.
27. Ye, Z., Wei, H., Soleimani, M. (2015). Resolution analysis using fully 3D electrical capacitance tomography. *Measurement*, 61, 270–279. DOI 10.1016/j.measurement.2014.10.060.
28. Taylor, S. H., Garimella, S. V. (2015). Shape-energy evolutionary reconstruction algorithm for electrical capacitance tomography in a high-aspect-ratio domain. *Sensors and Actuators A: Physical*, 233, 349–359. DOI 10.1016/j.sna.2015.07.019.
29. Ren, Z., Yang, W. (2015). A miniature two-plate electrical capacitance tomography sensor. *IEEE Sensors Journal*, 15(5), 3037–3049. DOI 10.1109/JSEN.2014.2383491.
30. Din, S. M., Razali, N. A., Pusppanathan, J., Song, C. P., Rahim, R. A. et al. (2017). Desktop tomography system using planar ECT device. *Telkomnika Telecommunication Computing Electronics and Control*, 15(2), 778–785. DOI 10.12928/telkomnika.v15i2.6116.
31. Tholin-Chittenden, C., Soleimani, M. (2017). Planar array capacitive imaging sensor design optimization. *IEEE Sensors Journal*, 17(24), 8059–8071. DOI 10.1109/JSEN.2017.2719579.